ELSEVIER

Journal of Structural Geology 28 (2006) 1640–1646

JOURNAL OF STRUCTURAL GEOLOGY

www.elsevier.com/locate/jsg

Numerical analysis of fold curvature using data acquired by high-precision GPS

Mark A. Pearce [a,*], Richard R. Jones [b,c], Steven A.F. Smith [d], Kenneth J.W. McCaffrey [b,d], Phill Clegg [d]

[a] *Department of Earth and Ocean Sciences, University of Liverpool, 4 Brownlow Street, Liverpool L69 3GP, UK*
[b] *Geospatial Research Ltd., Department of Earth Sciences, University of Durham, Durham DH1 3LE, UK*
[c] *e-Science Research Institute, University of Durham, Durham DH1 3LE, UK*
[d] *Reactivation Research Group, Department of Earth Sciences, University of Durham, Durham DH1 3LE, UK*

Received 17 December 2005; received in revised form 27 April 2006; accepted 2 May 2006
Available online 28 July 2006

Abstract

The maximum, minimum, Gaussian, and mean curvatures of a folded bedding surface are calculated from a high resolution data set. These data were collected using real-time kinematic (RTK) GPS and processed using commercially available software. The curvature parameters are calculated analytically from the first and second fundamental forms of the folded surface. Matrix algebra makes this method efficient for large data sets. Contoured maps of the curvature parameters can then be used as basemaps for the interpretation of other structural information such as fracture densities and orientations. This method provides precise analysis of folded surfaces in three dimensions and the data can be incorporated into larger-scale data sets obtained from seismic surveys.

Keywords: Curvature; Global Positioning System (GPS); Quantitative geological mapping

1. Introduction

Spatial variation in parameters such as principal, Gaussian, and mean curvatures has been used to examine the relationship between the geometry of folded surfaces and properties such as fracture density and orientation (Lisle, 1994; Fischer and Wilkerson, 2000; Hennings et al., 2000; Masaferro et al., 2003). Since these properties can strongly influence the permeability anisotropy of hydrocarbon reservoir rocks (Rawnsley et al., in press), analysis of fold curvature can give important insights during reservoir modelling (e.g. Stewart and Podolski, 1998). These curvature parameters can be calculated for a deformed bedding surface from data sets of three-dimensional geospatial measurements (Lisle, 1992, 1994; Bergbauer and Pollard, 2003a,b; Lisle and Martinez, 2005).

In this paper we describe the acquisition of spatial data from folded strata using high-precision Real-Time Kinematic (RTK) GPS, and show how these data can be used to calculate curvature parameters that describe the folded surface. Matrix algebra is used to process the large volumes of data collected using RTK GPS. This combination of innovative data collection and detailed data analysis using matrix algebra has the potential to refine reservoir models by increasing our understanding of quantitative geospatial relationships between folding and fracturing (Smith et al., in preparation).

Geometric analysis forms the basis of traditional fold classification (e.g. Fleuty, 1964; Ramsay, 1967; Hudleston, 1973; Ramsay and Huber, 1987) and is used to infer which mechanisms are most likely to have caused fold formation (e.g. Ramsay, 1967; Twiss and Moores, 1992; Hatcher, 1995; Mitra, 2003). Many of these classification schemes and analysis

* Corresponding author. Tel.: +44 151 7945201.
E-mail address: mark.pearce@liverpool.ac.uk (M.A. Pearce).

0191-8141/$ - see front matter © 2006 Elsevier Ltd. All rights reserved.
doi:10.1016/j.jsg.2006.05.010

techniques are only applicable in the 2D profile plane (e.g. dip isogons). Classification methods that consider deformation in the third dimension are generally qualitative, and consider idealised fold geometry (e.g. Williams and Chapman, 1979). Bergbauer and Pollard (2003a) have demonstrated how curvature analysis based on approximate mathematical descriptions of generalised fold geometries can lead to large errors when considering more complex areas of non-cylindrical folding. With the advent of spatially precise data sets such as those obtained by 3D seismic surveys or GPS (as used here), more quantitative analysis of 3D fold geometry is possible.

2. Methodology

2.1. Data collection

The RTK GPS data set used in this paper was collected from a single folded bedding surface (Fig. 1) in massively-bedded Dinantian limestones exposed on the foreshore at Howick, Northumberland, UK (Tucker, 1995). The rocks in this region have experienced heterogeneous transtensional deformation which has given rise to non-cylindrical periclinal folding and complex arrays of interlinked fracture sets (De Paola et al., 2005).

The RTK GPS system consists of pole-mounted differential GPS receivers (''rover units''), connected via a radio link to a static base station which continuously collects positional data from GPS satellites for the duration of the survey. Because RTK data collection is rapid, it is possible to measure large areas of folded bedding surfaces using a dense sampling grid. For each measurement position, the location, in 3D space, of the point is stored on the rover along with any attributes ascribed to that point (e.g. lithology, strike and dip of bedding, reference number). For our study at Howick, the data were collected with two rover units over two days and have a spacing of 30–50 cm between points. The typical spacing between points is determined by the size of the target structure and the level of detail required. In this case, the wavelength of the major fold in the surface is approximately 20 m, which can be accurately described by 40–50 points for each transect across the surface.

Fig. 1. Analysis of folded bedding surface at Howick, Northumberland, using RTK GPS. View looking south east.

As long as sufficient GPS satellites are in suitable orbits during the survey, the relative spatial precision of RTK measurements is normally better than 10 mm horizontally and 20 mm vertically. Spatial accuracy of the raw data within a global reference frame is significantly lower (typically 0.5 m). After completion of the survey, accuracy can be increased to match the level of precision by post-processing the data using standard correction files (Ordnance Survey Active RINEX and NASA precise ephemeris data). This post-processing allows multiple surveys collected over a number of days to be precisely matched to each other, and to be combined with other forms of geospatially referenced data using systems such as ArcGIS (Jones et al., 2004; McCaffrey et al., 2005a).

2.2. Curvature analysis

2.2.1. Defining curvature in three dimensions

In two-dimensions, the curvature, k, of a curve $z = f(x)$, is defined as follows

$$k = \frac{\dfrac{\mathrm{d}^2 z}{\mathrm{d}x^2}}{\left[1 + \left(\dfrac{\mathrm{d}z}{\mathrm{d}x}\right)^2\right]^{3/2}} \tag{1}$$

where z is the ordinate and x the abscissa (e.g. see Ramsay, 1967, pp. 346–347). Following this definition, crests and troughs are defined by the following equation:

$$\frac{\mathrm{d}z}{\mathrm{d}x} = 0 \tag{2}$$

(not $\mathrm{d}x/\mathrm{d}z = 0$ as shown erroneously by Ramsay, 1967, p. 347).

Curvature can be positive, negative or zero, denoting concave up (i.e. a trough), concave down (i.e. a crest), or flat structures, respectively. In 3D, at any given point on a surface there are an infinite number of directions through the point, each with its own curvature value. However, for each point, there are maximum (k_1) and minimum (k_2) curvature values and corresponding directions, called the principal curvature values and directions, respectively. Contouring values of k_1 to identify regions of high and low curvature provides a geometric basemap for analysis of attributes such as fracture density. It is also possible to test the correlation between the orientation of k_1 and k_2 and the orientation of these fracture sets. Two further parameters, the Gaussian and mean curvatures, fully describe the shape and orientation of folded surfaces, allowing dome, saddle and cylindrical forms to be distinguished (Lisle, 1994; Roberts, 2001; Bergbauer and Pollard, 2003a).

2.2.2. Refining data

The raw RTK data set was systematically collected by sampling along an approximate grid. It is not necessary to use a precisely spaced regular grid because the data are easily re-gridded using a variety of commercially available software packages. This saves time in the data collection stage. Care was taken to ensure that the point spacing of both the raw and re-gridded data was much smaller than the wavelength of the structures analysed, and that there were no high-amplitude minor structures that would distort the analysis. We created a surface from the data set using basic interpolation functionality in GoCAD® (Mallet, 1992); comparable functionality exists in many alternative tools. This step helps to smooth small-scale irregularities in the data, and will not introduce spurious geometrical features in the interpolated surface as long as grid spacing is small. The surface is then re-sampled along an x and y grid to give equally spaced points in both directions. The x and y positions of these new points, together with each corresponding z (height) value, were exported and used as an input file for a Matlab® program which was used to calculate the curvature parameters.

2.2.3. Calculating curvature

The method of calculating curvature used here is mathematically analogous to that used by Bergbauer and Pollard (2003a). However, it is novel in its use of matrix algebra to deal with the large data sets acquired using RTK GPS.

For a surface,

$$\mathbf{r} = \begin{bmatrix} x \\ y \\ z(x,y) \end{bmatrix} \tag{3}$$

two orthogonal tangents to the surface are given by the partial derivatives of the surface in orthogonal directions

$$\frac{\partial \mathbf{r}}{\partial x} = \mathbf{r}_x = \begin{bmatrix} 1 \\ 0 \\ \dfrac{\partial z}{\partial x} \end{bmatrix} \tag{4}$$

and

$$\frac{\partial \mathbf{r}}{\partial y} = \mathbf{r}_y = \begin{bmatrix} 0 \\ 1 \\ \dfrac{\partial z}{\partial y} \end{bmatrix} \tag{5}$$

These are used to calculate the matrix of the first fundamental form of the surface, $\mathbf{I}$ (Henderson, 1998, p. 80).

$$\mathbf{I} = \begin{bmatrix} \mathbf{r}_x \cdot \mathbf{r}_x & \mathbf{r}_x \cdot \mathbf{r}_y \\ \mathbf{r}_x \cdot \mathbf{r}_y & \mathbf{r}_y \cdot \mathbf{r}_y \end{bmatrix} \tag{6}$$

The second fundamental form, which describes the rate of change of the normal to the surface as a function of position (Bergbauer and Pollard, 2003a,b), can also be described by a matrix composed of second partial derivatives. Because the matrix describes the rate of change of the normal to the surface (i.e. the normal curvature), the second partial derivatives are dotted with the unit normal to the plane which contains the two tangent vectors (the tangent plane). The unit normal is found using two of the derivatives already calculated by dividing the cross product of the two vectors (which gives the normal vector) by its magnitude:

$$\hat{\mathbf{n}} = \frac{\dfrac{\partial \mathbf{r}}{\partial x} \times \dfrac{\partial \mathbf{r}}{\partial y}}{\left| \dfrac{\partial \mathbf{r}}{\partial x} \times \dfrac{\partial \mathbf{r}}{\partial y} \right|} \tag{7}$$

This cross product function is usually a defined function within any matrix based mathematics program (e.g. Matlab or Mathematica) but it should be noted that the determinant of the cross product of these two vectors can be found by:

$$\left| \frac{\partial \mathbf{r}}{\partial x} \times \frac{\partial \mathbf{r}}{\partial y} \right| = \sqrt{|\mathbf{I}|} \tag{8}$$

The matrix of the second fundamental form, $\mathbf{II}$, is (Henderson, 1998, p. 129):

$$\mathbf{II} = \begin{bmatrix} \dfrac{\partial^2 \mathbf{r}}{\partial x^2} \cdot \hat{\mathbf{n}} & \dfrac{\partial^2 \mathbf{r}}{\partial x \partial y} \cdot \hat{\mathbf{n}} \\ \dfrac{\partial^2 \mathbf{r}}{\partial x \partial y} \cdot \hat{\mathbf{n}} & \dfrac{\partial^2 \mathbf{r}}{\partial y^2} \cdot \hat{\mathbf{n}} \end{bmatrix} \tag{9}$$

There is a linear map (a transformation in which every element is mapped to one other element of the same dimensionality, e.g. lines are mapped to lines), $\mathbf{L}$, which maps tangent space to itself. This map is known in differential geometry as the shape operator and has several properties which are useful in determining the various curvature parameters described earlier.

$$\mathbf{L} = \mathbf{I}^{-1}\mathbf{II} \tag{10}$$

This is analogous to Eq. (9) of Bergbauer and Pollard (2003a).

The normal curvature, k_v in a particular direction, v, is defined as a combination of the two tangent vectors described in Eqs. (4) and (5), and is given by:

$$k_v = \mathbf{L}(\mathbf{v}) \cdot \mathbf{v} \tag{11}$$

where

$$\mathbf{v} = a\frac{\partial \mathbf{r}}{\partial x} + b\frac{\partial \mathbf{r}}{\partial y} \tag{12}$$

and

$$\mathbf{L}(\mathbf{v}) = c\frac{\partial \mathbf{r}}{\partial x} + d\frac{\partial \mathbf{r}}{\partial y} \tag{13}$$

and where

$$\begin{bmatrix} c \\ d \end{bmatrix} = \mathbf{L}\begin{bmatrix} a \\ b \end{bmatrix} \tag{14}$$

describes the relationship between the coefficients of Eqs. (12) and (13).

More importantly, for the reasons discussed above, the maximum and minimum principal curvature directions (k_1 and k_2) and magnitudes can be found by taking the eigenvectors and eigenvalues of **L**.

The Gaussian curvature, G, is the product of the two principal curvature values and is also given by the determinant of **L**.

$$G = k_1 k_2 = |\mathbf{L}| \tag{15}$$

The mean curvature, M, is the mean of k_1 and k_2 and is also half the trace (sum of the diagonal elements) of **L**.

2.2.4. Implementation and checking

When processing the data from Howick, the first partial derivative for each data point was calculated by taking the mean of the dips of the two edges connecting the point to its adjacent grid vertices, in the appropriate positive and negative directions. This could then be repeated for the second partial derivatives using the same method but with the dips of the edges as input rather than the positions of the vertices themselves. The relatively simple matrix operations used in this method were written into Matlab® code which generates an output file returning the x, y, z positions and the various curvature parameters for each point. Our script was checked using synthetically generated folds for which analytical solutions could be calculated. The error between the analytically calculated values for the curvature of the synthetic folds and those derived using matrix algebra was <1%. This is a very small error which when combined with the precision of the real data set gives the ability to analyse the curvature of small-scale folds in a quantitative way with very high accuracy. As a final check, normal and Gaussian curvature values for the Howick folds were compared graphically with curvature functionality in Midland Valley's *3-D Move* software (http://www.mve.com/Home/Software/3DMove).

3. Results

Maps of the maximum curvature magnitude and maximum and minimum curvature directions are shown in Fig. 2a, b and c respectively. The Gaussian curvature of the sampled surface is shown in Fig. 2d. The maps of curvature properties can be draped onto the folded surface and examined further using 3D visualisation software (Fig. 2e).

3.1. Features highlighted by the maximum principal curvature

Plotting the magnitude of the maximum principal curvature (Fig. 2a) highlights antiformal and synformal regions. Plotting absolute magnitude of curvature (i.e. ignoring whether values are positive or negative) can often be useful, for example in showing the spatial distribution of regions where fold tightness is greatest. By also plotting the maximum principal curvature direction (Fig. 2b), it is possible to see how the direction of the maximum curvature changes over the surface. It is not necessary to plot both the maximum and minimum principal curvatures on the same plot because by definition these are perpendicular. Plotting the direction of the maximum principal curvature is most useful to highlight variations in the orientation of the fold profile plane, whilst plots of the direction of the minimum principal curvature allow the position of fold hinges to be tightly constrained (Fig. 2c).

In the data set from Howick, the main region of maximum curvature is in the south-western part of the surveyed surface. Here there are two regions of high absolute curvature, one positive and one negative; these highlight a synform–antiform pair. The area between these two hinges represents a short limb within the asymmetric fold sequence. The overall decrease in absolute curvature magnitude northwards shows that the surface flattens out and that the fold is not cylindrical. Traditionally, these two geometric properties can make it difficult to delineate the hinge precisely, and to differentiate between the hinge and the crest of the fold. The mathematically defined properties calculated with this data set allow hinge lines to be constructed by picking points of highest curvature across a transect, then following the directions of minimum curvature (k_2) from these points (Fig. 2c). Since k_1 and k_2 are perpendicular, the hinge lines will always be perpendicular to k_1 and can therefore be accurately defined, even within areas where the hinge lines are not readily identifiable at the outcrop.

3.2. Features highlighted by the Gaussian curvature

Whilst the maximum curvature shows regions where the folding is tightest, it may also be useful to identify the area of highest 3D strain (Lisle, 1994; Lisle and Martinez, 2005; Smith et al., in preparation). This can be constrained by the Gaussian curvature calculated according to Eq. (15). The areas of highest maximum principal curvature at the southern end of the folded surface are also highlighted by the Gaussian curvature (Fig. 2d) as being a dome and basin pair ($G > 0$).

Another property of the Gaussian curvature is to highlight the inflection points of the fold (Lisle, 1999). In 2D fold analysis, this is where the curvature changes from being positive to negative and is, therefore, zero (Ramsay, 1967, pp. 346–347). When considering 3D folds, there will be very few areas where there is zero curvature in any direction. However, because the Gaussian curvature is a product of the two principal curvatures it only requires one of the principals to be 0. For curvilinear folds, where one of the principal curvatures is 0, the fold is undergoing an inflection. Once these points are identified, they can then be joined to highlight mathematically defined inflection lines (Fig. 2c).

4. Discussion

4.1. Small-scale RTK data sets

Newly developed methods of field study that allow quantitative analysis of outcrop-scale structures are now able to provide new insights at critical sub-seismic scales (Jones et al.,

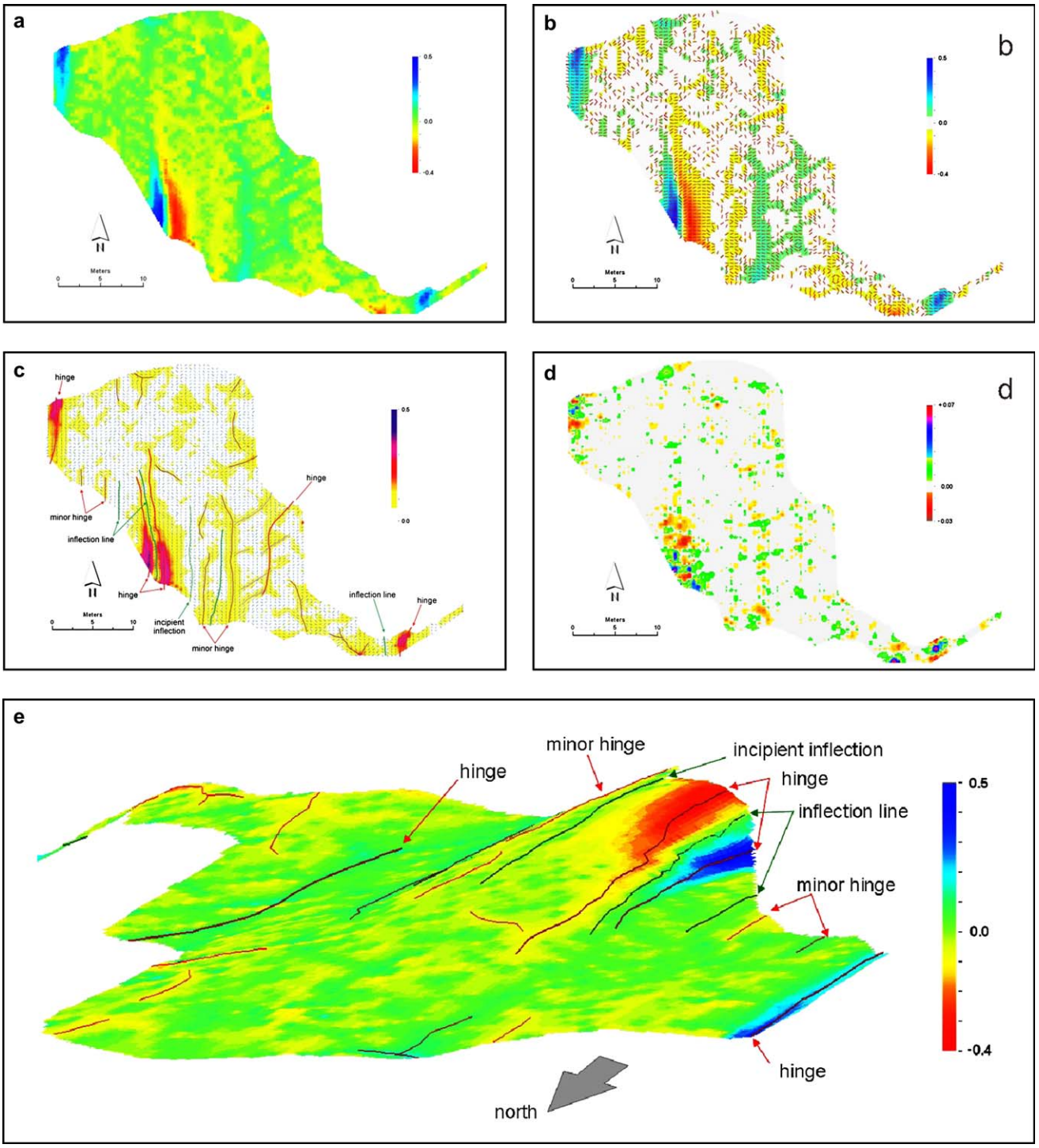

Fig. 2. Results of curvature analysis from folded bedding surface at Howick: (a) map of variation in magnitude of normal curvature; (b) map showing variation in the direction of maximum principal curvature, superimposed on the magnitude of normal curvature (for clarity, curvature values close to zero [$-0.05 < k_v < +0.05$] are not shown); (c) map showing variation in the direction of minimum principal curvature, superimposed on the *absolute* magnitude of maximum principal curvature, with interpreted hinge and inflection lines shown; (d) map of Gaussian curvature; (e) 3D perspective view of curvature values draped onto the fold with interpreted hinge and inflection lines (vertical exaggeration $\times 1.5$). Units of curvature are m^{-1}.

2004; McCaffrey et al., 2005a,b). In this way, the analysis of meso-scale fold curvature presented in this paper complements previous examples of curvature analysis, which were based on seismic-scale data with a maximum resolution of 20 m (e.g. Stewart and Wynn, 2000) or on gridded data sets obtained from regional structure contour maps (Lisle, 1994; Bergbauer and Pollard, 2003a). A common problem is that it can sometimes be difficult to quantify the uncertainty and precision in these data sets (Jones et al., 2004). Bergbauer and Pollard (2003a) used a contour spacing of 100 feet and a data set of approximately 480 points which is an order of magnitude fewer than our new data set. Whilst this is sufficient to

highlight the large scale structure, there may be many other scales of structure which contribute to the bulk properties of the rocks (Stewart and Podolski, 1998; Stewart and Wynn, 2000). With a densely sampled, high-precision data set, smaller scale structures can be imaged and analysed, and then the data set can be smoothed to examine larger wavelength structures. The information about the sub-seismic scale deformation of the rocks can then be incorporated into data sets for which similar analyses have been carried out at seismic resolution.

4.2. Method of calculating curvature and data display

The method used to calculate the various curvature parameters in this paper is based on the mathematics presented by Bergbauer and Pollard (2003a), but offers an alternative implementation based on matrix algebra (thus reducing the need for complex equations involving differential calculus). Software specially optimised for this type of mathematics (e.g. Matlab®) makes recovery of eigenvalues simple, and in general is particularly well suited to the efficient analysis of large data sets (e.g. 10^5–10^7 points), including those collected using other methods of digital data acquisition such as terrestrial laser-scanning (Jones et al., 2004; Clegg et al., 2005).

Results of curvature analysis can easily be imported and displayed in a variety of GIS software and 3D visualisation packages. The raw data points can easily be embedded within larger-scale digital elevation data sets to provide high resolution models of areas of interest. Using other digital data collection technologies (McCaffrey et al., 2005a; Wilson et al., 2005) an entire virtual outcrop (Clegg et al., 2005; Trinks et al., 2005) can be created showing different aspects of interest from the same geological region.

Maps created by analysing intrinsic properties of geological surfaces can serve as basemaps for other types of data (e.g. fracture density and orientation) which can influence bulk rock properties (e.g. permeability and seismic anisotropy). These data can be collected using conventional field methods such as line transects or identified from georeferenced laser scan data sets (Smith et al., in preparation). Comparing geometric data and physical properties enables identification of systematic spatial variations in the latter with respect to the former. Relating these sub-seismic to regional-scale structures (Clegg et al., 2005; Trinks et al., 2005) provides reservoir modellers with improved fracture data to enhance estimates of permeability.

5. Conclusion

In this paper, we propose a mathematically efficient solution to calculate curvature from high density and high-precision data sets collected using equipment such as RTK GPS. This method, facilitated by matrix algebra using commercially available software, calculates the maximum and minimum principal, Gaussian, and mean curvatures. These provide the basis for a complete characterisation of the geometry of folded surfaces and allow some application of traditional 2D attributes to 3D folds. As a result of this quantitative analysis, further studies of the relationship between fracturing and the geometry of deformed rocks will be possible, leading to a better understanding of the physical properties of the rock volume.

Acknowledgements

Thanks to Richard Lisle and Kieran Mulchrone for constructive and helpful reviews, and to Ian Mynatt and Dave Pollard for a correction to an equation in an earlier version of the manuscript. Field work for this project was supported by a Nuffield Foundation Undergraduate Bursary (SAFS). Dr. Sheila Carter of the University of Leeds, School of Mathematics is thanked for discussion regarding curvature. Parts of this work relate to NERC Follow-on Fund (NE/C506964/1), and Ocean Margins Link project (NER/T/S/2000/01018), funded by Statoil UK Ltd, BP and NERC. RRG thanks Midland Valley Exploration for non-commercial licences of 3D-Move.

References

Bergbauer, S., Pollard, D.D., 2003a. How to calculate normal curvatures of sampled geological surfaces. Journal of Structural Geology 25, 277–289.

Bergbauer, S., Pollard, D.D., 2003b. Erratum to "How to calculate normal curvatures of sampled geological surfaces". Journal of Structural Geology 25, 2167.

Clegg, P., Trinks, I., McCaffrey, K.J.W., Holdsworth, R.E., Jones, R.R., Hobbs, R., Waggott, S., 2005. Towards the virtual outcrop. Geoscientist 15 (1), 8–9.

De Paola, N., Holdsworth, R.E., McCaffrey, K.J.W., Barchi, M.R., 2005. Partitioned transtension: an alternative to basin inversion models. Journal of Structural Geology 27, 607–625.

Fischer, M.P., Wilkerson, M.S., 2000. Predicting the orientation of joints from fold shape: results of pseudo-three-dimensional modelling and curvature analysis. Geology 28, 15–18.

Fleuty, M.J., 1964. The description of folds. Proceedings of the Geologists' Association 75, 461–492.

Hatcher, R.D., 1995. Structural Geology: Principles, Concepts, and Problems, second ed. Prentice Hall, New Jersey, USA, 525 pp.

Henderson, D.W., 1998. Differential Geometry: A Geometric Introduction. Prentice Hall, 250 pp.

Hennings, P.H., Olson, J.E., Thompson, L.B., 2000. Combining outcrop data and three-dimensional structural models to characterise fractured reservoirs: an example from Wyoming. AAPG Bulletin 84, 830–849.

Hudleston, P.J., 1973. Fold morphology and some geometrical implications of theories of fold development. Tectonophysics 12, 415–430.

Jones, R.R., McCaffrey, K.J.W., Wilson, R.W., Holdsworth, R.E., 2004. Digital field data acquisition: towards increased quantification of uncertainty during geological mapping. In: Curtis, A., Wood, R. (Eds.), Geological Prior Information. Geological Society, Special Publication 239, pp. 43–56.

Lisle, R.J., 1992. Constant bed-length folding: three-dimensional geometrical implications. Journal of Structural Geology 14, 245–252.

Lisle, R.J., 1994. Detection of zones of abnormal strains in structures using Gaussian curvature analysis. AAPG Bulletin 78, 1811–1819.

Lisle, R.J., 1999. The 3D geometry of folds: problems and solutions. Abstracts with Programs – Geological Society of America, 1999 Annual Meeting.

Lisle, R.J., Martinez, J.L.F., 2005. Structural analysis of seismically mapped horizons using the developable surface model. AAPG Bulletin 89, 839–848.

Mallet, J.L., 1992. GOCAD: a computer aided design program for geological applications. In: Turner, A.K. (Ed.), Three-dimensional Modeling with Geoscientific Information Systems. NATO ASI Series C: Mathematical and Physical Sciences 354, 123–141.

Masaferro, J.L., Bulnes, M., Poblet, J., Casson, N., 2003. Kinematic evolution and fracture prediction of the Valle Morado structure inferred from 3D seismic data, Salta Province, northwest Argentina. AAPG Bulletin 87, 1083–1104.

McCaffrey, K.J.W., Jones, R.R., Holdsworth, R.E., Wilson, R.W., Clegg, P., Imber, J., Holliman, N., Trinks, I., 2005a. Unlocking the spatial dimension: digital technologies and the future of geoscience fieldwork. Journal of the Geological Society, London 162, 1–12.

McCaffrey, K.J.W., Holdsworth, R.E., Imber, J., Clegg, P., De Paola, N., Wilson, R.W., Jones, R.R., Hobbs, R., Holliman, N., Trinks, I., 2005b. Putting the geology back into Earth models. EOS 86, 461–466.

Mitra, S., 2003. A unified kinematic model for the evolution of detachment folds. Journal of Structural Geology 25, 1659–1673.

Ramsay, J.G., 1967. Folding and Fracturing of Rocks. McGraw-Hill, New York, 568 pp.

Ramsay, J.G., Huber, M.I., 1987. Folds and Fractures. In: The Techniques of Modern Structural Geology, vol. 2. Academic Press, London.

Rawnsley, K., de Keijzer, M., Wei, L., Bettembourg, S., Asyee, W., Massaferro, L., Swaby, P., Drysdale, D., Boettcher, D. Characterising fracture and matrix heterogeneities in folded Devonian carbonate thrust sheets, Waterton tight gas fields, Western Canada. In: Lonergan, L., Jolley, R. (Eds.), Fractured Reservoirs. Geological Society of London, Special Publication, in press.

Roberts, A., 2001. Curvature attributes and their application to 3D interpreted horizons. First Break 19, 85–100.

Stewart, S.A., Podolski, R., 1998. Curvature analysis of gridded geological surfaces. In: Coward, M.P., Daltaban, T.S., Johnson, H. (Eds.), Structural Geology in Reservoir Characterisation. Geological Society, Special Publication 127, pp. 133–147.

Stewart, S.A., Wynn, T.J., 2000. Mapping spatial variation in rock properties in relationship scale-dependent structure using spectral curvature. Geology 28, 691–694.

Trinks, I., Clegg, P., McCaffrey, K.J.W., Jones, R.R., Hobbs, R., Holdsworth, R.E., Holliman, N., Imber, J., Waggott, S., Wilson, R., 2005. Mapping and analysing virtual outcrops. Visual Geosciences, doi:10.1007/s10069-005-0026-9.

Tucker, M., 1995. Carboniferous rocks of the Howick shore section. In: Scrutton, C. (Ed.), Northumbrian Rocks and Landscape: A Field Guide, second ed. Yorkshire Geological Society, pp. 81–91.

Twiss, R.J., Moores, E.M., 1992. Structural Geology. WH Freeman & Co., New York, 532 pp.

Williams, G.D., Chapman, T.J., 1979. The geometrical classification of non-cylindrical folds. Journal of Structural Geology 1, 181–186.

Wilson, R.W., McCaffrey, K.J.W., Jones, R.R., Imber, J., Clegg, P., Holdsworth, R.E., 2005. Lofoten has its faults! Detailed fault analysis and 3D digital mapping in the Norway's Lofoten Islands. Geoscientist 15 (2), 4–9.